

Comprehensive computational model of Earth's ring current

M.-C. Fok

Universities Space Research Association, NASA Goddard Space Flight Center, Greenbelt, Maryland

R. A. Wolf and R. W. Spiro

Physics and Astronomy Department, Rice University, Houston, Texas

T. E. Moore

Laboratory for Extraterrestrial Physics, NASA Goddard Space Flight Center, Greenbelt, Maryland

Abstract. A comprehensive ring current model (CRCM) has been developed that couples the Rice Convection Model (RCM) and the kinetic model of Fok and coworkers. The coupled model is able to simulate, for the first time using a self-consistently calculated electric field, the evolution of an inner magnetosphere plasma distribution that conserves the first two adiabatic invariants. The traditional RCM calculates the ionospheric electric fields and currents consistent with a magnetospheric ion distribution that is assumed to be isotropic in pitch angle. The Fok model calculates the plasma distribution by solving the Boltzmann equation with specified electric and magnetic fields. To combine the RCM and the Fok model, the RCM Birkeland current algorithm has been generalized to arbitrary pitch angle distributions. Given a specification of height-integrated ionospheric conductance, the RCM component of the CRCM computes the ionospheric electric field and currents. The Fok model then advances the ring current plasma distribution using the electric field computed by the RCM and at the same time calculates losses along particle drift paths. We present the logic of CRCM and the first validation results following the H⁺ distribution during the previously studied magnetic storm of May 2, 1986. The H⁺ fluxes calculated by the coupled model agree very well with observations by AMPTE/CCE. In particular, the coupled model is able to reproduce the high H⁺ flux seen on the dayside at $L \sim 2.3$ that the previous simulation, which employed a Stern-Volland convection model with shielding factor 2, failed to produce. Though the Stern-Volland and CRCM electric fields differ in several respects, the most notable difference is that the CRCM predicts strong electric fields near Earth in the storm main phase, particularly in the dusk-midnight quadrant. Thus the CRCM injects particles more deeply and more quickly.

1. Introduction

The terrestrial ring current is a large-scale electrical current system encircling Earth's magnetic equator at typical radial distances of 2 to 8 Earth radii (R_E). The current is carried principally by westward drifting trapped ions in the 1–300 keV energy range [e.g., *Daglis et al.*, 1999]. During magnetic storms and substorms the ring current can be greatly strengthened when bursts of intense electric field transport ions from the plasma sheet and outer ring current earthward and energize them. The enhanced ring current produces a global geomagnetic disturbance and significantly contributes to the magnetic depression on Earth's surface as measured by the *Dst* index [*Rostoker*, 1972], which is widely used to identify the growth and decay of magnetic storms. During the recovery phase of a magnetic storm, the ring current decreases via various processes, e.g., charge exchange with the neutral atmosphere, interactions with plasma waves, and Coulomb collisions with the plasmasphere. Eventually, the magnetic

storm energy stored in the ring current is deposited into the underlying ionosphere and atmosphere.

Numerous theoretical models have been developed to study the ring current and its aeronomical effects [e.g., *Chen et al.*, 1993, 1994; *Fok et al.*, 1993, 1996, 1999; *Fok and Moore*, 1997; *Jordanova et al.*, 1996, 1997]. Most of these models take into account loss processes along particle drift paths and consider full pitch angle distributions, but all of them employ electric and magnetic field models that are not computed self-consistently with the plasma distribution. The Rice Convection Model (RCM), on the other hand, utilizes a sophisticated method of calculating electric fields in the ionosphere-magnetosphere system, consistent with the particle distribution in the magnetosphere [*Harel et al.*, 1981]. However, the RCM calculates drifts on the basis of an assumed isotropic pitch angle distribution.

Motivated by the well-known strengths and deficiencies of ring current models and by the desire to calculate ring current plasma distributions self-consistently, we have developed a comprehensive ring current model (CRCM) by combining the RCM and Fok's kinetic model. Both the RCM and the Fok model set their grids in the ionosphere and place the high-latitude boundary in the auroral zone. The traditional RCM assumes pitch angle isotropy, while the Fok model assumes

conservation of the first and the second adiabatic invariants. In order to couple with the Fok model, the RCM algorithm for calculating Birkeland current has been generalized to arbitrary pitch angle distributions. Given a specification of ionospheric conductance and initial ring current distribution, the RCM component of the CRCM computes the ionospheric electric field and currents. The Fok model then advances the plasma distribution using the electric field computed by the RCM and at the same time calculates particle losses along drift paths. The updated distributions are then returned to the RCM to complete the computation cycle. In brief, the RCM serves as an electric field solver in the CRCM and the Fok model plays the role of a particle tracer. This combined model includes major loss mechanisms and complete pitch angle distribution and at the same time considers electric coupling between the ionosphere and the magnetosphere. In the following sections we will present the detailed model logic of CRCM and the first validation results following the H⁺ distribution during the previously studied magnetic storm of May 2, 1986.

2. Generalized RCM for Anisotropic Distributions

The RCM is an algorithm for calculating the distribution of magnetospheric particles (above ~1 keV) as well as the electrostatic potential, and magnetic-field-aligned current in the closed-field-line region of the magnetosphere. Although an early version of the RCM pictured all magnetospheric particles as mirroring at the equatorial plane [Jaggi and Wolf, 1973], the model has generally used a formalism that assumes that the particles are isotropic [Harel et al., 1981; Wolf, 1983]. The RCM implicitly assumes that the particles are subject to a pitch angle scattering process that randomizes pitch angles in a time small compared to a drift period without changing particle energy. This is the simplest reasonable assumption for the plasma sheet, which is observed to have a basically isotropic distribution [Stiles et al., 1978]. The plasma sheet ion distribution is apparently kept isotropic because of chaotic orbits [e.g., Sergeev et al., 1993], but the isotropy assumption is clearly inaccurate for the ring current region.

Effects of electron loss are often included in the RCM [e.g., Erickson et al., 1991; Wolf et al., 1991] in terms of their effect on ionospheric conductance and on the total number of particles in each flux tube, but the loss-cone-associated anisotropy is assumed to affect a small range of pitch angles, and the net drift of the particles is still computed under the assumption of isotropy. Ion loss has generally not been included in past RCM runs.

For the usual case of an isotropic distribution function, RCM particles are characterized by an energy invariant λ_j , where

$$W_j = \lambda_j V^{-2/3}. \quad (1)$$

W_j is the kinetic energy of the particle, including gyromotion and bounce motion, and V is the volume of a magnetic flux tube containing one unit of magnetic flux [Harel et al., 1981; Wolf, 1983]. (The particle drift velocity is assumed to be much smaller than the gyration and bounce velocities.) A given subset of particles j is characterized by a given chemical species (electrons, H⁺ ions, sometimes O⁺ ions) and given

energy invariant λ_j . The bounce-averaged drift velocity is given by

$$\mathbf{v}_D = \frac{\mathbf{E} \times \mathbf{B}}{B^2} + \frac{\mathbf{B} \times \nabla W_j}{q_j B^2}. \quad (2)$$

In the ionosphere the electric field in (2) is normally assumed to be a potential field, for timescales more than a few minutes. In the magnetosphere, where the magnetic field changes significantly with time, \mathbf{E} has both potential and inductive terms. The equation for advancing the particle distribution is

$$\left(\frac{\partial}{\partial t} + \mathbf{v}_D \cdot \nabla \right) \eta_j = -\frac{\eta_j}{\tau_j}, \quad (3)$$

where η_j is the number of particles of type j per unit magnetic flux and τ_j is the loss lifetime. The number density $n_j = \eta_j/V$. The MHD pressure is expressed in terms of RCM parameters λ_j and η_j as

$$P = \frac{2}{3} V^{-5/3} \sum_j \lambda_j \eta_j. \quad (4)$$

Starting from a distribution of magnetospheric particles, the RCM calculates the Birkeland current into the ionosphere from the Vasyliunas [1970] equation, which can be written as

$$\frac{J_{\parallel i}}{B_i} = \frac{\hat{\mathbf{b}} \cdot \nabla V \times \nabla P}{B}, \quad (5)$$

where $J_{\parallel i}$ is the current per unit area parallel to \mathbf{B}_i ; positive current is down into the ionosphere, and both hemispheres are counted together; B_i is the magnetic field strength in the ionosphere at those locations, with symmetry assumed between the two hemispheres; $\hat{\mathbf{b}}$ is a unit vector along \mathbf{B} . The right side of (5) is constant along a field line and can therefore be evaluated anywhere along the line. Substituting (1) and (4) in (5) we can reexpress the Vasyliunas equation in terms of RCM variables [Wolf, 1983]:

$$\frac{J_{\parallel i}}{B_i} = \frac{1}{B} \sum_j \hat{\mathbf{b}} \cdot (\nabla \eta_j \times \nabla W_j). \quad (6)$$

The RCM calculates the distribution of ionospheric potential Φ by solving

$$\nabla \cdot (-\bar{\Sigma} \cdot \nabla \Phi) = J_{\parallel i} \sin I, \quad (7)$$

where $\bar{\Sigma}$ is a tensor representing ionospheric Hall and Pedersen conductance (both hemispheres together); I is the magnetic dip angle. Sometimes a neutral-wind term is added to (7) [e.g., Spiro et al., 1988]. The ionospheric conductance is generally taken from a background model that includes ionization by sunlight and some kind of auroral enhancement model. Once the ionospheric potential distribution is calculated by solution of (7), that distribution is mapped along magnetic field lines to the equatorial plane, where it is used in the calculation of the drift velocity. The major inputs to the RCM are the magnetic field model, the conductance model, the initial and outer boundary plasma distributions, and the potential distribution on the outer (high- L) boundary.

We need to modify the Vasyliunas equation [(5) or (6)] for the case where the pressure tensor is gyrotropic but not isotropic. Heinemann [1990] used anisotropic fluid theory to derive a generalized Vasyliunas equation for a gyrotropic

plasma, and *Birmingham* [1992] used kinetic theory to derive another form. However, neither of those is convenient to use in the CRCM, which follows bounce-averaged drifts. We therefore derive another form from drift theory, for the case where the particle distributions are characterized by the invariants M and K instead of λ_j , and M and K are assumed to be conserved as a particles drifts. The bounce-averaged gradient curvature (GC) drift velocity is given by [Wolf, 1983]

$$\mathbf{v}_{GC} = \frac{\mathbf{B} \times \nabla W_j(M, K, \mathbf{x})}{q_j B^2}, \quad (8)$$

where M is the first adiabatic invariant and

$$K = \int_{s_{ms}}^{s_{mn}} \sqrt{B_m - B(s)} ds. \quad (9)$$

Here B_m is the magnetic field at the mirror point and s_{mn} and s_{ms} are the Northern and Southern hemisphere mirror points, respectively. In the case of zero-parallel electric field, K is related to the second adiabatic invariant, J by $K = J / \sqrt{8m_0 M}$ [Roederer, 1970]. [Note the strong resemblance between (8) and the gradient/curvature drift part of (2)]. Equation (8) is valid anywhere on a field line. We adopt the bookkeeping convention of mapping all magnetospheric particles along field lines to the equatorial plane. The current per unit length in that plane due to particles of type j is given by

$$\mathbf{j}_{GC,j,E} = (\eta_j B_E) q_j \mathbf{v}_{GC,j,E} = \eta_j \hat{\mathbf{b}}_E \times \nabla_E W_j, \quad (10)$$

where B_E is the equatorial magnetic field and $\eta_j B_E$ is the number of particles of type j per unit area in the equatorial plane, and we have used (8) in establishing the second equality. By equating $J_{||}/B$ in the ionosphere to $-(\nabla \cdot \mathbf{j}_{GC})_E / B_E$ we obtain, from (10),

$$\begin{aligned} \frac{j_{||i}}{B_i} &= \frac{1}{B_E} \sum_j \hat{\mathbf{b}}_E \cdot \nabla_E \eta_j \times \nabla_E W_j(M, K, \mathbf{x}) \\ &= \frac{1}{B} \sum_j \hat{\mathbf{b}} \cdot \nabla \eta_j \times \nabla W_j(M, K, \mathbf{x}). \end{aligned} \quad (11)$$

Note the similarity between (6) and (11). The expression after the last equal sign in (11) can be evaluated anywhere on the field line. In the new coupled code the equations are solved in the ionosphere, where the magnetic field is assumed to be a dipole. The downward Birkeland current per unit area on an ionospheric shell of radius r_i (6500 km) is given by

$$J_{||} = \frac{1}{r_i^2 \cos l_i} \sum_j \left(\frac{\partial \eta_j}{\partial l_i} \frac{\partial W_j}{\partial \phi_i} - \frac{\partial \eta_j}{\partial \phi_i} \frac{\partial W_j}{\partial l_i} \right), \quad (12)$$

where l_i and ϕ_i are ionospheric latitude and local time.

3. Coupling Fok's Kinetic Model With the Generalized RCM

The Fok kinetic model calculates the temporal variation of the phase space density of a particle species s , by solving the following bounce-averaged Boltzmann transport equation:

$$\frac{\partial \bar{f}_s}{\partial t} + \langle \dot{l}_i \rangle \frac{\partial \bar{f}_s}{\partial l_i} + \langle \dot{\phi}_i \rangle \frac{\partial \bar{f}_s}{\partial \phi_i} = -\nu \sigma_s \langle n_H \rangle \bar{f}_s - \left(\frac{\bar{f}_s}{0.5\tau_b} \right)_{\text{loss cone}} \quad (13)$$

where $\bar{f}_s = \bar{f}_s(t, l_i, \phi_i, M, K)$ is the average distribution function on the field line between mirror points, l_i is the magnetic latitude at the ionospheric location of the geomagnetic field line, σ_s is the cross section for charge exchange of species s with the neutral hydrogen, n_H is the hydrogen density, and τ_b is the bounce period. The second term on the right-hand side of (13) is applied only to particles with pitch angles inside the loss cone, which is defined at ~ 100 km altitude. This study includes only loss due to charge exchange with neutral hydrogen and to the loss cone.

In the Fok model the motion of the particles is described by their drifts across field lines that are labeled by their ionospheric foot points. The shape of a field line may change, but the ionospheric foot points are assumed to be fixed and essentially dipolar. The bounce-averaged drift velocities, $\langle \dot{l}_i \rangle$ and $\langle \dot{\phi}_i \rangle$, can be expressed as [Fok and Moore, 1997]

$$\begin{aligned} \langle \dot{l}_i \rangle &= -\frac{1}{q\xi} \frac{\partial H}{\partial \phi_i}, \\ \langle \dot{\phi}_i \rangle &= \frac{1}{q\xi} \frac{\partial H}{\partial l_i}, \end{aligned} \quad (14)$$

where $\xi = M_E \sin(2l_i)/r_i$ and M_E is the Earth's magnetic dipole moment. The Hamiltonian H is given by

$$H = W + q\Phi - q\Omega \frac{M_E}{2r_i} \cos 2l_i, \quad (15)$$

where Ω is the angular velocity of the rotation of the Earth itself and W is the particle kinetic energy which is a function of M and K . The derivatives of the first, second, and third terms on the right-hand side of (15) correspond to the geomagnetic gradient curvature drift, electric drift (convection), and corotation [e.g., Fok and Moore, 1997], respectively, of a charged particle.

To couple the Fok model and the RCM, the phase space density obtained from (13) has to be converted to the RCM variable η_j , which represents the number of particles per unit magnetic flux in the range $\Delta M \Delta K$. We show in the appendix that the η_j associated with a range $\Delta M \Delta K$ is related to the distribution function by

$$\eta_j = 4\sqrt{2\pi m_0}^{3/2} \bar{f}_s M_j^{1/2} \Delta M_j \Delta K_j. \quad (16)$$

For a given initial plasma distribution \bar{f}_s , we calculate the corresponding η_j and apply the generalized RCM algorithm to calculate the ionosphere potential Φ . We then calculate particle drifts $\langle \dot{l}_i \rangle$ and $\langle \dot{\phi}_i \rangle$ using (14). The particle distribution is advanced by solving (13) to complete the computation cycle.

4. Simulated H⁺ Distribution During the Storm on May 2, 1986

We have tested the performance of the CRCM by simulating the previously studied magnetic storm of May 2, 1986 [Fok et al., 1996]. On that day the Active Magnetospheric Particle Tracer Explorers/Charge Composition Explorer (AMTPE/CCE) crossed the ring current region on two orbits, traversing the postmidnight and prenoon sectors. The first orbit (~ 0500 UT) was before the storm onset. The second orbit was near the end

of the storm main phase at ~ 2000 UT when Dst reached ~ -80 nT. The charge-energy-mass (CHEM) instrument on CCE measured differential fluxes of H^+ and other ions in the energy range of 1–300 keV/q. Fok et al. [1996] calculated the H^+ fluxes during this storm using their ring current model assuming a dipolar magnetic field and a Stern-Volland type convection $[\Phi = \Phi_0(\sin^2\theta_p/\sin^2\theta_i)^\gamma \sin(\phi_i - \phi_{\text{offset}})]$ [Volland, 1973; Stern, 1975] with shielding factor $\gamma = 2$ and $\phi_{\text{offset}} = 2$ hours. The values of γ and ϕ_{offset} were chosen to best fit the CHEM measurements. In general, the simulations agreed very well with the observations, except that the model failed to reproduce the observed high H^+ fluxes on the dayside at $L \sim 2.3$.

We have revisited the storm on May 2, 1986, and simulated the H^+ fluxes using the CRCM. The simulation region in the ionosphere is set from 44.5° to 67.2° magnetic latitude. We assume the potential at the poleward boundary has the form $\Phi_p = \Phi_0 \sin\phi_i$, with Φ_0 changing according to instantaneous Kp value. Here Φ_0 (in kV) is assumed to be 2.0, 3.3, 5.5, 9.2, 15, 24, 37, 51, 61, 61 corresponding to $Kp = 0, 1, \dots, 9$ [Maynard and Chen, 1975]. The RCM conductance model superimposes a Hardy et al. [1987] auroral enhancement on a background conductance based on the MSIS neutral atmosphere [Hedin, 1991], the IRI-90 ionospheric model [Bilitza et al., 1993], and collision-frequency expressions given by Riley [1994]. The magnetic field is assumed to be a dipole, because in this study we consider only the inner magnetosphere at $L < 7$. The initial distribution at 0200 UT was taken from the H^+ fluxes seen by CCE/CHEM during quiet periods of the mission [Sheldon and Hamilton, 1993]. The H^+ fluxes at $L = 6.8$ measured by CCE/CHEM at ~ 0800 and 2400 UT on May 2, 1986, are used as boundary conditions, which are assumed to be independent of local time. The instantaneous boundary fluxes are obtained by linear interpolation in UT. In summary, the magnetic field model, the initial H^+ fluxes, and the boundary fluxes are the same as those used by Fok et al. [1996]. The distinct difference of this study from Fok et al. [1996] is the use of the RCM electric field in place of the Stern-Volland analytic electric field model.

Plate 1a shows the CRCM simulated equatorial fluxes during the storm at three times that are labeled in the Kp plot (top panel). Plate 1c shows the corresponding fluxes using the Stern-Volland electric field. The H^+ energy distribution is color coded as shown in the color wheel (Plate 1, top right), with red brightness representing low-energy (1–5 keV) flux, green representing medium-energy (5–40 keV) flux, and blue representing high-energy (40–300 keV) flux. The color bars show the scale of the brightness of each color. In this visualization, yellow signifies the existence of low- and medium-energy ions but lack of high-energy particles. Similarly, magenta represents a mix of low- and high-energy plasmas with deficiency of particles at medium energies. White indicates that the average fluxes in all three energy ranges are above the flux scale limit, which is $5 \times 10^5 \text{ cm}^{-2} \text{ s}^{-1} \text{ sr}^{-1} \text{ keV}^{-1}$ in Plate 1. The corresponding convection field potential contours (in kV) calculated by the CRCM are plotted in Plate 1b, while the Stern-Volland patterns are shown in Plate 1d.

Plate 1a, part 1 represents the prestorm quiet time distribution [Sheldon and Hamilton, 1993]. Owing to the long charge exchange lifetimes of high-energy H^+ , the inner ring current consists primarily of protons with energy ≥ 100 keV (blue color) that have slowly diffused in from higher L shells.

This population does not change noticeably during the 1-day main phase of the storm. The outer ring current, on the other hand, contains mainly the low- to medium-energy H^+ (orange color) drifting sunward from the plasma sheet. The transition region in between is a mixture of low- and high-energy ions (magenta ring). The convection field is weak at this time (Plate 1a, part 1).

At 1100 UT (Plate 1a-1d, part 2), convection becomes stronger and the potential drop across the simulation boundary is ~ 45 kV. The convection electric field pushes ions earthward on the nightside (the bright yellow band). The green-blue area on the dusk side is not quickly accessible to plasma sheet H^+ ions of < 5 keV. Similarly, the magenta-blue area is the forbidden region for medium-energy (5–40 keV) ions. The blue "teardrop" is the overlap of these two regions. Neither low- nor medium-energy ions from the plasma sheet can penetrate into this region at this time. Near the end of the main phase at 2300 UT (Plate 1a-1d, part 3), the potential drop across the simulation region reaches 100 kV. The strong convection field causes deep penetration of the freshly injected plasma sheet ions. The forbidden region of the low-energy H^+ (green-cyan color) is confined into a small teardrop shape region with a long spiral tail sweeping from the evening sector to noon. The corresponding region for medium-energy ions is even smaller, with a relatively short tail sweeping across noon to postdawn.

Comparisons between fluxes computed from the RCM and Stern-Volland electric fields show both similarities and differences.

1. The flux plots in column 1, 1 hour after the start of the run, are nearly the same, because the runs started from the same initial flux; the weak convection fields, operating only for an hour, have only had a mild effect on the fluxes.

2. In column 2, representing the situation 9 hours after the start and in the midst of the initial injection, the RCM brings fresh ions (light colors) closer to Earth in the postmidnight sector than the Stern-Volland model does, because the RCM's inner magnetospheric westward electric field is stronger in that sector.

3. In column 2, fresh, medium-energy ions have swept farther westward around the dayside in the RCM run than with Stern-Volland, mainly because of the different boundary conditions on the potentials in the two cases. The Stern-Volland potential, for this particular case, is symmetric about a line between 1400 and 0200 local time, while the boundary potential in the RCM case is symmetric about the noon-midnight line. The 2-hour rotation in the Stern-Volland potential was chosen to optimize agreement with CCE data. That rotation is qualitatively consistent with the conclusion of Gussenhoven et al. [1981]. Consequently, in the Stern-Volland run, ions that drifted around the duskside tended to be swept out of the magnetosphere before reaching local noon, while in the RCM case, they could drift farther west. However, note that the near-Earth region of the RCM potential patterns does exhibit an eastward rotation similar to the Stern-Volland patterns. This rotation occurs naturally in the RCM as a result of the day-night asymmetry in ionospheric conductance [Wolf, 1970] and the tendency for the region 2 Birkeland currents to rotate the pattern near the Earth [e.g., Wolf, 1983; Senior and Blanc, 1984].

4. In column 3, representing a time near the end of the main phase, the inner edge of the freshly injected particles is closer to Earth in the RCM run than in the Stern-Volland case. The

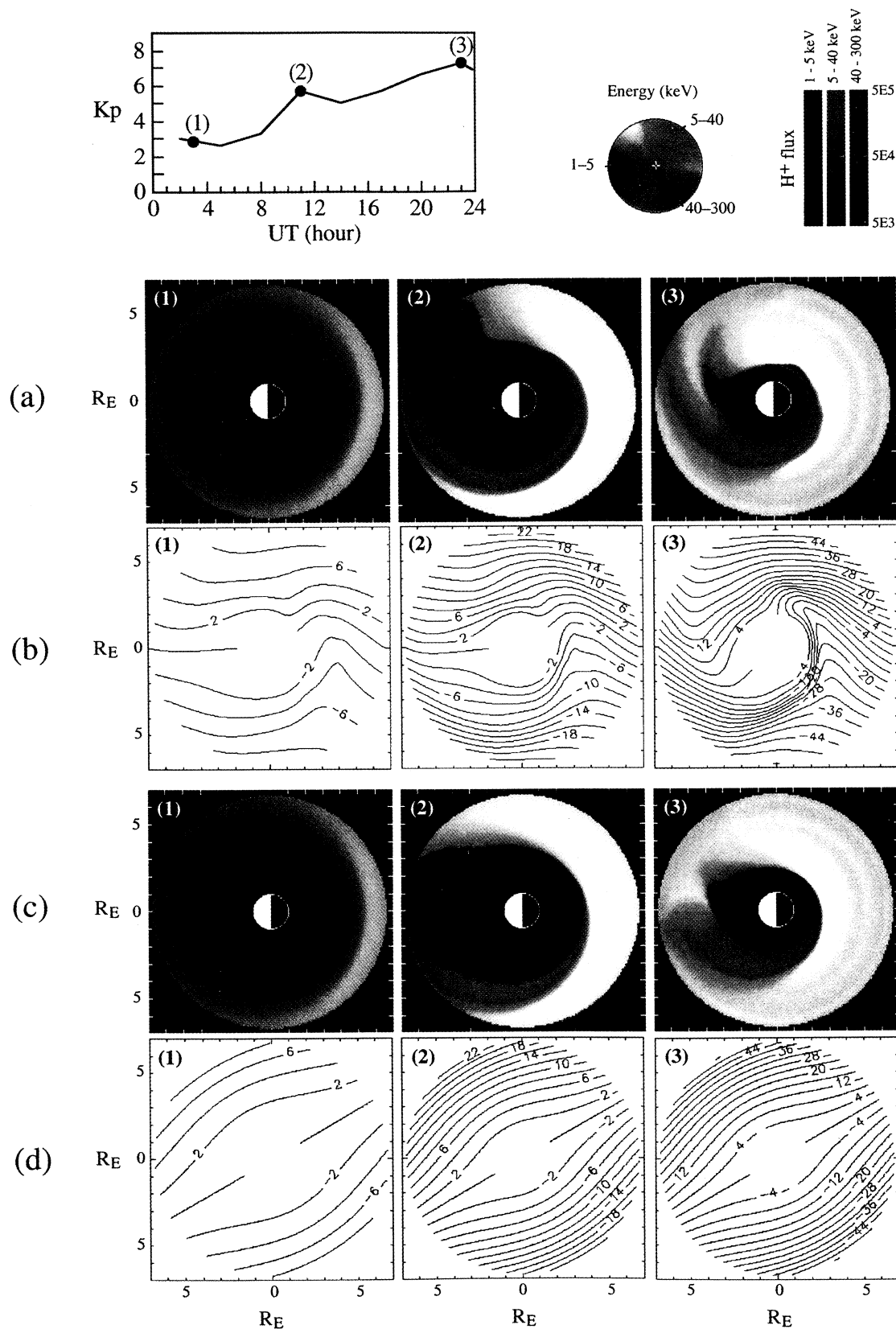


Plate 1. Top panel: K_p values on May 2, 1986. (a): Calculated H^+ flux in $\text{cm}^{-2} \text{s}^{-1} \text{sr}^{-1} \text{keV}^{-1}$ at the equator at times labeled on the K_p plot. Ions with low energies (1–5 keV), medium energies (5–40 keV), and high energies (40–300 keV) are represented by red, green, and blue, respectively. (b): potential contours in kV calculated by the Rice Convection Model (RCM) module of the comprehensive ring current model (CRCM). (c): same as Plate 1a, except calculated using the Stern-Volland model. (d): same as Plate 1b, except calculated using the Stern-Volland model. Noon is to the left in Plates 1a-1d.

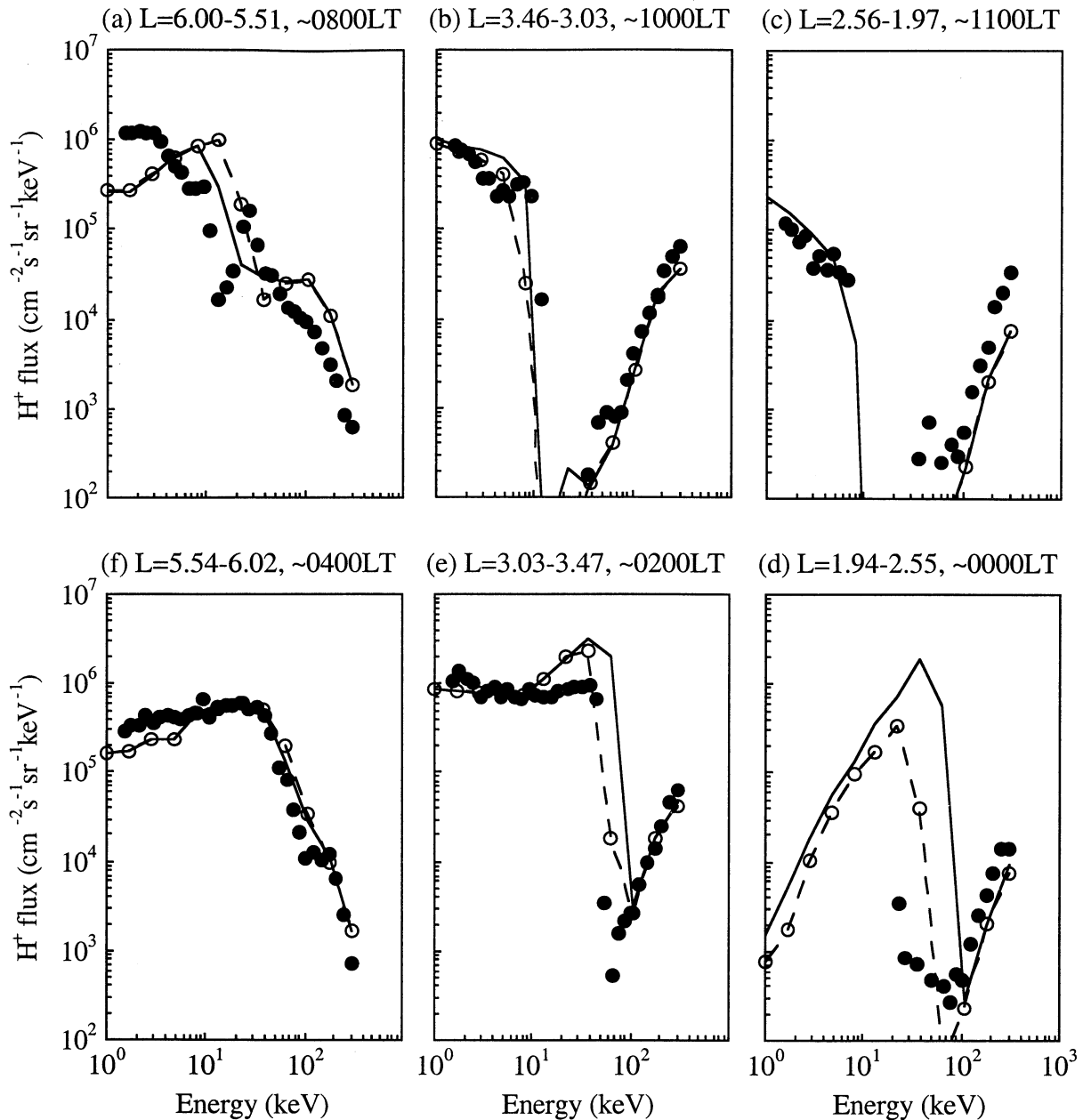


Figure 1. Simulated pitch-angle-averaged H^+ fluxes at six locations near the end of the storm main phase on May 2, 1986, at (a) 0800 LT, (b) 1000 LT, (c) 1100 LT, (d) 0000 LT, (e) 0200 LT, and (f) 0400 LT. Dashed lines with open circles are fluxes calculated with Stern-Volland type convection. Solid lines are fluxes calculated with RCM convection field. The corresponding CCE/CHEM measurements are shown by solid circles.

basic reason is that the electric fields at low L are generally stronger in the RCM than in the Stern-Volland model. Late in the main phase, the RCM developed a region of particularly strong outward field at $L \sim 3$ in the dusk-midnight quadrant. This feature is typical of the RCM in conditions of strong convection; it appears to be the same feature that was noted by Rowland and Wygant [1998] and Burke *et al.* [1998] in CRRES electric field data for major storms. On the duskside the plasma sheet ions, which generate the region 2 Birkeland currents, penetrate closer to Earth than the electrons, which control ionospheric conductance. In the dusk-midnight sector, region 2 currents tend to flow down into a region of the ionosphere that does not have a strongly enhanced conductance, and

strong electric fields are required to drive ionospheric currents poleward through the low-conductance zone to the region of strong electron precipitation. This is basically the mechanism proposed by Southwood and Wolf [1978] to explain subauroral ion drift events, but the region of enhanced electric field becomes broader in latitude during strong convection, when the inner edge of the plasma sheet electrons is strongly eroded by precipitation losses. (See Garner [2000] or Sazykin [2000] for a more complete discussion.)

Figure 1 shows the comparison of the pitch-angle-averaged H^+ fluxes near the end (2000–2300 UT) of May 2, 1986, calculated by the two simulations. Energy spectra are shown at six locations along the CCE orbit. Dashed lines with open

circles are results from the Fok model with Stern-Volland convection. These fluxes are slightly different from those displayed in Figure 3 of Fok *et al.* [1996], because the previously published results were calculated with the spatial grid at the equator and with different numerical approaches. Solid lines are results from the CRCM. The corresponding CCE measurements (solid circles) are also plotted in Figure 1. As shown in the figure, both runs give similar results in the outer ring current (Figures 1a and 1f). However, at $L < 3.5$, CRCM always produces higher fluxes than the old model, consistent with the fact that the RCM predicts a stronger inner magnetospheric convection electric field than the Stern-Volland model does. The most remarkable difference between the two simulations is found in Figure 1c. The CRCM successfully reproduces the high H^+ fluxes at low energy seen by CCE/CHEM at $L \sim 2.3$ at 1100 LT, while the Stern-Volland convection field fails to produce low-energy flux at the observed level. This result amply illustrates that the electric connection between the ionosphere and the magnetosphere allows deep penetration of plasma sheet plasmas during geomagnetic active periods. However, CRCM tends to overestimate ion fluxes on the nightside in the inner ring current region (Figures 1d and 1e). The inaccuracy in the ionospheric conductance model and the potential at the poleward boundary are possible causes of this discrepancy.

5. Summary

We have developed a comprehensive computational model of the Earth's ring current that follows the evolution of the ring current plasma while conserving the first two adiabatic invariants in a self-consistently calculated electric field, the comprehensive ring current model (CRCM).

1. The CRCM couples the Rice Convection Model and the Fok kinetic model. It combines the strengths of the two parent models and includes most of the important physics of the ring current.

2. The CRCM is the first ring current model that considers arbitrary ion pitch angle distributions and computes the electric coupling between the ionosphere and the magnetosphere.

3. The CRCM has been used to simulate the main phase of the magnetic storm on May 2, 1986. There was excellent agreement with particle measurements made during the storm. In particular, CRCM reproduces the observed high fluxes of keV protons at the inner edge of the dayside ring current. Previous simulation which applied the Stern-Volland convection model failed to produce fluxes at the observed levels at this energy and location, owing to the oversimplified representation of electric field penetration from outer to inner magnetosphere.

The merging of these two well-developed models should provide a powerful tool for advancing understanding of ring current dynamics, the role of the ionosphere in the ring current development, and solar wind control of the ring current.

Appendix: Relationship Between f and η

The total number of particles per unit magnetic flux is given by

$$\eta_{\text{total}} = \int \frac{ds}{B} \int \bar{f} d^3 p = \int \frac{ds}{B} \int_0^\infty \int_0^\infty \bar{f} 4\pi p_\perp dp_\perp d|p_\parallel|. \quad (\text{A1})$$

We have used the fact that $f(-p_\parallel, p_\perp) = f(p_\parallel, p_\perp)$. It is convenient to integrate over just the magnitude of p_\parallel , because we are going to convert this to an integral over M and K , and neither of these quantities distinguishes the sign of p_\parallel . Doing this conversion using the Jacobian gives

$$dMdK = \left\| \begin{array}{cc} \frac{\partial M}{\partial p_\perp} & \frac{\partial M}{\partial |p_\parallel|} \\ \frac{\partial K}{\partial p_\perp} & \frac{\partial K}{\partial |p_\parallel|} \end{array} \right\| dp_\perp d|p_\parallel|. \quad (\text{A2})$$

The derivatives are all taken at a specific position. Since

$$M = \frac{p_\perp^2}{2m_o B}, \quad (\text{A3})$$

we have

$$\frac{\partial M}{\partial p_\perp} = \frac{p_\perp}{m_o B}, \quad \frac{\partial M}{\partial |p_\parallel|} = 0 \quad (\text{A4})$$

The Jacobian derivative $\partial K/\partial |p_\parallel|$ is taken at constant p_\perp at a point on the field line:

$$\left(\frac{\partial K}{\partial |p_\parallel|} \right)_{p_\perp} = \frac{dK}{dB_m} \left(\frac{\partial B_m}{\partial |p_\parallel|} \right)_{p_\perp} = \frac{dK}{dB_m} \frac{|p_\parallel|}{m_o M}. \quad (\text{A5})$$

Substituting (A4) and (A5) in (A2) gives

$$dMdK = \frac{dK}{dB_m} \frac{p_\perp |p_\parallel|}{m_o^2 MB} dp_\perp d|p_\parallel|. \quad (\text{A6})$$

Substituting (A6) in (A1), the integral over the flux tube reduces to $\int ds/|p_\parallel|$, and many factors cancel out. The result is

$$\eta_{\text{total}} = 4\sqrt{2}\pi m_o^{3/2} \iint \bar{f} M^{1/2} dMdK. \quad (\text{A7})$$

The η associated with a range $\Delta M \Delta K$, which is the typical η in the RCM, is related to the distribution function by

$$\eta_j = 4\sqrt{2}\pi m_o^{3/2} \bar{f} M_j^{1/2} dM_j dK_j. \quad (\text{A8})$$

Acknowledgments. The authors are grateful to Frank Toffoletto and Trevor Garner for helpful conversations and frequent technical assistance. This work was supported by the NASA Office of Space Science by grant NAG5-4968 to the University Space Research Association and grant NAG5-4267 to Rice University.

Janet G. Luhmann thanks Michael Heinemann and Janet U. Kozyra for their assistance in evaluating this paper.

References

- Bilitza, D., K. Rawer, L. Bosny, and T. Gulyaeva, International Reference Ionosphere - Past, present, future, *Adv. Space Res.*, (13), 3-23, 1993.
- Birmingham, T. J., Birkeland currents in an anisotropic, magnetostatic plasma, *J. Geophys. Res.*, 97, 3907-3917, 1992.
- Burke, W. J., N. C. Maynard, M. P. Hagan, R. A. Wolf, G. R. Wilson, L. C. Gentile, M. S. Gussenhoven, C. Y. Huang, T. W. Garner, and F. J. Rich, Electrodynamics of the inner magnetosphere observed in the dusk sector by CRRES and DMSP during the magnetic storm of June 4-6, 1991, *J. Geophys. Res.*, 103, 29,399-29,418, 1998.
- Chen, M. W., M. Schulz, L. R. Lyons, and D. J. Gorney, Stormtime transport of ring current and radiation belt ions, *J. Geophys. Res.*, 98, 3835-3849, 1993.
- Chen, M. W., L. R. Lyons, and M. Schulz, Simulations of phase space distributions of storm time proton ring current, *J. Geophys. Res.*, 99, 5745-5759, 1994.
- Daglis, I. A., R. M. Thorne, W. Baumjohann, and S. Orsini, The terrestrial ring current: Origin, formation, and decay, *Rev. Geophys.*, 37, 407-438, 1999.

- Erickson, G. M., R. W. Spiro, and R. A. Wolf, The physics of the Harang discontinuity, *J. Geophys. Res.*, **96**, 1633-1645, 1991.
- Fok, M.-C., and T. E. Moore, Ring current modeling in a realistic magnetic field configuration, *Geophys. Res. Lett.*, **24**, 1775-1778, 1997.
- Fok, M.-C., J. U. Kozyra, A. F. Nagy, C. E. Rasmussen, and G. V. Khazanov, Decay of equatorial ring current ions and associated aeronomical consequences, *J. Geophys. Res.*, **98**, 19,381-19,393, 1993.
- Fok, M.-C., T. E. Moore, and M. E. Greenspan, Ring current development during storm main phase, *J. Geophys. Res.*, **101**, 15,311-15,322, 1996.
- Fok, M.-C., T. E. Moore, and D. C. Delcourt, Modeling of inner plasma sheet and ring current during substorms, *J. Geophys. Res.*, **104**, 14,557-14,569, 1999.
- Garner, T. W., A case study of the June 4-5, 1991 magnetic storm using the Rice convection model, Ph. D. thesis, Rice Univ., Houston, Tex., 2000.
- Gussenhoven, M. S., D. A. Hardy, and W. J. Burke, DMSP/F2 electron observations of equatorward auroral boundaries and their relationship to magnetospheric electric fields, *J. Geophys. Res.*, **86**, 768-778, 1981.
- Hardy, D. A., M. S. Gussenhoven, R. Raistrick, and W. J. McNeil, Statistical and functional representations of the pattern of auroral energy flux, number flux, and conductivity, *J. Geophys. Res.*, **92**, 12,275-12,294, 1987.
- Harel, M., R. A. Wolf, P. H. Reiff, R. W. Spiro, W. J. Burke, F. J. Rich, and M. Smiddy, Quantitative simulation of a magnetospheric substorm, 1, Model logic and overview, *J. Geophys. Res.*, **86**, 22,17-22,41, 1981.
- Hedin, A. E., Extension of the MSIS thermospheric model into the middle and lower atmosphere, *J. Geophys. Res.*, **96**, 1159-1172, 1991.
- Heinemann, M., Representations of currents and magnetic fields in anisotropic magnetohydrostatic plasma, *J. Geophys. Res.*, **95**, 7789-7798, 1990.
- Jaggi, R. K., and R. A. Wolf, Self-consistent calculation of the motion of a sheet of ions in the magnetosphere, *J. Geophys. Res.*, **78**, 2852-2866, 1973.
- Jordanova, V. K., L. M. Kistler, J. U. Kozyra, G. V. Khazanov, and A. F. Nagy, Collisional losses of ring current ions, *J. Geophys. Res.*, **101**, 111-126, 1996.
- Jordanova, V. K., J. U. Kozyra, A. F. Nagy, and G. V. Khazanov, Kinetic model of the ring current-atmosphere interactions, *J. Geophys. Res.*, **102**, 14,279-14,291, 1997.
- Maynard, N. C., and A. J. Chen, Isolated cold plasma regions: Observations and their relation to possible production mechanisms, *J. Geophys. Res.*, **80**, 1009-1013, 1975.
- Riley, P., Electrodynamics of the low latitude ionosphere, Ph. D. thesis, Rice Univ., Houston, Tex., 1994.
- Roederer, J. G., *Dynamics of Geomagnetically Trapped Radiation*, Springer-Verlag, New York, 1970.
- Rostoker, G., Geomagnetic indices, *Rev. Geophys.*, **10**, 935-950, 1972.
- Rowland, D. E., and J. R. Wygant, Dependence of the large-scale, inner magnetospheric electric field on geomagnetic activity, *J. Geophys. Res.*, **103**, 14,959-14,964, 1998.
- Sazykin, S., Theoretical studies of penetration of magnetospheric electric fields to the ionosphere, Ph. D. thesis, Utah State Univ., Logan, Utah, 2000.
- Senior, C., and M. Blanc, On the control of magnetospheric convection by the spatial distribution of ionospheric conductivities, *J. Geophys. Res.*, **89**, 261-284, 1984.
- Sergeev, V. A., M. Malkov, and K. Mursula, Testing the isotropic boundary algorithm method to evaluate the magnetic field configuration in the tail, *J. Geophys. Res.*, **98**, 7609-7620, 1993.
- Sheldon, R. B., and D. C. Hamilton, Ion transport and loss in the Earth's quiet ring current, 1, Data and standard model, *J. Geophys. Res.*, **98**, 13,491-13,508, 1993.
- Southwood, D. J., and R. A. Wolf, An assessment of the role of precipitation in magnetospheric convection, *J. Geophys. Res.*, **83**, 5227-5232, 1978.
- Spiro, R. W., R. A. Wolf, and B. G. Fejer, Penetration of high-latitude-electric-field effects to low latitudes during SUNDIAL 1984, *Ann. Geophys.*, **6**, 39-50, 1988.
- Stern, D. P., The motion of a proton in the equatorial magnetosphere, *J. Geophys. Res.*, **80**, 595-599, 1975.
- Stiles, G. S., E. W. Hones Jr., S. J. Bame, and J. R. Asbridge, Plasma sheet pressure anisotropies, *J. Geophys. Res.*, **83**, 3166-3172, 1978.
- Vasyliunas, V. M., Mathematical models of magnetospheric convection and its coupling to the ionosphere, in *Particles and Fields in the Magnetosphere*, edited by B. McCormac, pp. 60-71, D. Reidel, Norwell, Mass., 1970.
- Volland, H., A semiempirical model of large-scale magnetospheric electric fields, *J. Geophys. Res.*, **78**, 171-180, 1973.
- Wolf, R. A., Effects of ionospheric conductivity on convective flow of plasma in the magnetosphere, *J. Geophys. Res.*, **75**, 4677-4698, 1970.
- Wolf, R. A., The quasi-static (slow-flow) region of the magnetosphere, in *Solar Terrestrial Physics*, edited by R. L. Carovillano and J. M. Forbes, pp. 303-368, D. Reidel, Norwell, Mass, 1983.
- Wolf, R. A., R. W. Spiro, and F. J. Rich, Extension of the Rice Convection Model into the high-latitude ionosphere, *J. Atmos. Terr. Phys.*, **53**, 817-829, 1991.

M.-C. Fok and T. E. Moore, NASA Goddard Space Flight Center, Code 692, Greenbelt, MD 20771. (mei-ching.fok@gsfc.nasa.gov)
 R. W. Spiro and R. A. Wolf, Physics and Astronomy Department, Rice University, Houston, TX 77005.

(Received June 21, 2000; revised September 19, 2000; accepted September 19, 2000.)